JBC RESEARCH ARTICLE

Temperature instability of a mutation at a multidomain junction in Na,K-ATPase isoform ATP1A3 (p.Arg756His) produces a fever-induced neurological syndrome

Received for publication, July 1, 2022, and in revised form, November 18, 2022 Published, Papers in Press, December 1, 2022,
https://doi.org/10.1016/j.jbc.2022.102758

Elena Arystarkhova[1,*], Mads S. Toustrup-Jensen[2,‡], Rikke Holm[2,‡], Jae-Kyun Ko[3], Kyung Eun Lee[3], Polina Feschenko[1], Laurie J. Ozelius[4], Allison Brashear[5], Bente Vilsen[2], and Kathleen J. Sweadner[1,*]

From the [1]Department of Neurosurgery, Massachusetts General Hospital, Boston, Massachusetts, USA; [2]Department of Biomedicine, Aarhus University, Aarhus C, Denmark; [3]Department of Surgery, The Ohio State University Wexner Medical Center, Columbus, Ohio, USA; [4]Department of Neurology, Massachusetts General Hospital, Boston, Massachusetts, USA; [5]Department of Neurology, Jacobs School of Medicine and Biomedical Sciences, Buffalo, New York, USA

Edited by Ursula Jakob

ATP1A3 **encodes the α3 isoform of Na,K-ATPase. In the brain, it is expressed only in neurons. Human *ATP1A3* mutations produce a wide spectrum of phenotypes, but particular syndromes are associated with unique substitutions. For arginine 756, at the junction of membrane and cytoplasmic domains, mutations produce encephalopathy during febrile infections. Here we tested the pathogenicity of p.Arg756His (R756H) in isogenic mammalian cells. R756H protein had sufficient transport activity to support cells when endogenous ATP1A1 was inhibited. It had half the turnover rate of wildtype, reduced affinity for Na^+, and increased affinity for K^+. There was modest endoplasmic reticulum retention during biosynthesis at 37 °C but little benefit from the folding drug phenylbutyrate (4-PBA), suggesting a tolerated level of misfolding. When cells were incubated at just 39 °C, however, α3 protein level dropped without loss of β subunit, paralleled by an increase of endogenous α1. Elevated temperature resulted in internalization of α3 from the surface along with some β subunit, accompanied by cytoplasmic redistribution of a marker of lysosomes and endosomes, lysosomal-associated membrane protein 1. After return to 37 °C, α3 protein levels recovered with cycloheximide-sensitive new protein synthesis. Heating *in vitro* showed activity loss at a rate 20- to 30-fold faster than wildtype, indicating a temperature-dependent destabilization of protein structure. Arg756 appears to confer thermal resistance as an anchor, forming hydrogen bonds among four linearly distant parts of the Na,K-ATPase structure. Taken together, our observations are consistent with fever-induced symptoms in patients.**

Mutations in *ATP1A3*, the gene that encodes the isoform of Na,K-ATPase that is expressed in most neurons in the nervous system, cause an extraordinarily wide range of syndromes. Syndromes can manifest in utero with developmental malformation, at birth with intractable epilepsy, in infancy with paroxysmal motor symptoms, or later in life with persistent symptoms triggered by stress or febrile infection. The majority of mutations are missense and heterozygous. A clinical continuum of symptoms can be traced, but there is a strong bias for some substitutions to produce a particular syndrome. Symptom severity does not correlate with residual Na,K-ATPase activity (1–3), and so broader investigation is needed to determine the underlying mechanisms. In prior work comparing mutations from mild (rapid-onset dystonia-parkinsonism, RDP) and severe perinatal phenotypes, we showed evidence that protein with severe mutations was retained in endoplasmic reticulum and that the unfolded protein response (UPR) was elicited (3). The syndrome in patients with mutations of Arg756 (to His, Leu, or Cys) is distinct from most other ATP1A3 syndromes because symptoms do not manifest until triggered by fever. Patients make substantial recovery over weeks, but there are persistent RDP-like symptoms that accrue with additional febrile episodes.

The first crystal structure of a P-type ATPase (that of SERCA1, the skeletal muscle sarcoplasmic-endoplasmic reticulum Ca^{2+}-ATPase, ATP2A1) demonstrated that the corresponding arginine residue, R751, is part of an important network of hydrogen bonds [Fig. 8 of reference (4)]. It was predicted to play the same role in Na,K-ATPase [called R758 in reference (5)]. It is on the cytoplasmic portion of the longest transmembrane span, M5, and its side chain is extended and makes contact with backbone atoms (carbonyls) of surrounding protein segments. The residue is strongly conserved in the P2A, P2B, and P2C subgroups of P-type ATPases [See A P-type ATPase database (traplabs.dk)]. Fig. 1 shows Na,K-ATPase R756 (ATP1A3 numbering) in three different conformational states on the left.

The properties and roles of the Na,K-ATPase isoforms are well-studied (6). Crystal structures of ATP1A1 (Na,K-ATPase α1) are useful to investigate relationships among conserved residues because the three Na,K-ATPase isoforms are 89% identical, and their sequence differences are mostly in patches

‡ These authors contributed equally to this work.
* For correspondence: Kathleen J. Sweadner, sweadner@helix.mgh.harvard.edu; Elena Arystarkhova, aristarkhova@helix.mgh.harvard.edu.

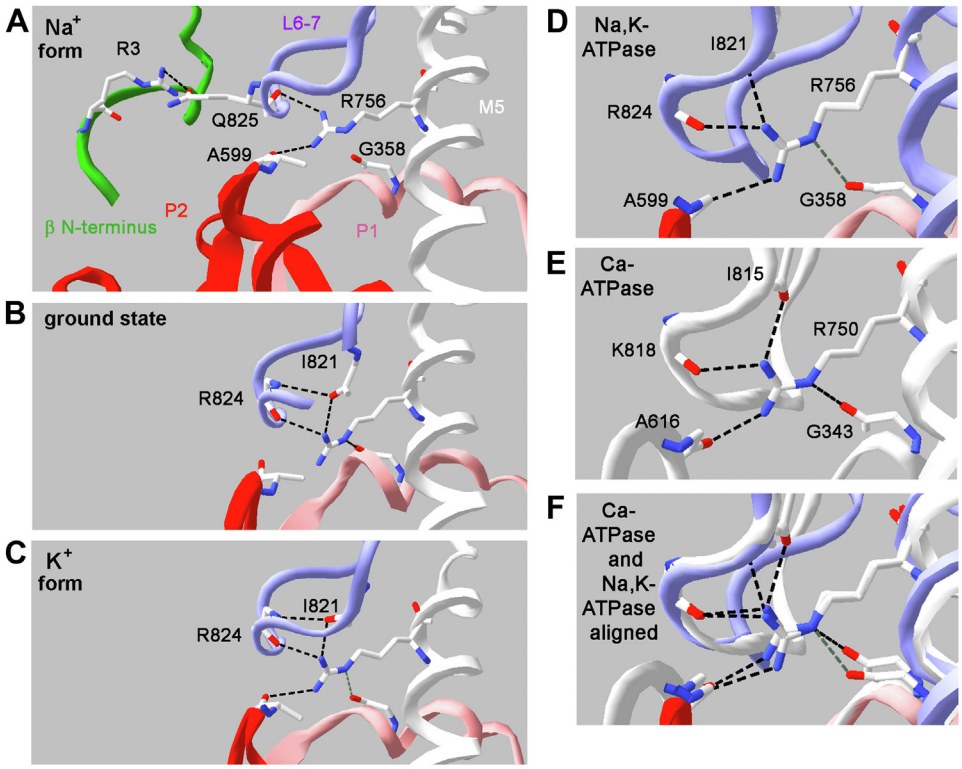

Figure 1. R756 helps connect four domains of Na,K-ATPase α and the β subunit. *A–C*, Portions of crystal structures of α1β1 Na,K-ATPase in three different conformation states are illustrated with different colors (*ribbon representation*). In the order of the linear structure, the P domain is made in two parts (*pink and red*) that are interrupted by the 214-amino acid N domain (not visible). M5 is a long transmembrane span, but the portion shown is its cytoplasmic extension (*white*). The cytoplasmic loop between M6 and M7 is *lavender*, and the N terminus of the β subunit is *green*. The backbone and sidechains of R756 and Q825 of α3 are shown in *stick format*, but only the backbone carbonyls and amides of Glu358, Ala599, Ile821, and Arg824 are shown, because the latter's sidechains are not involved in the hydrogen bonds. Not illustrated: The arginine is further surrounded by hydrophobic residues in L6-7. ATP1A3 residues I821, M822, and P826 are all close contacts (<4.2 Å) of the R756 side chain, and the stem of the R824 side chain runs antiparallel with that of R756. In the ground state structure, a portion of L6-7 is cut away to make the backbone of I821 more visible. Putative hydrogen bonds (*black dashed lines*) were calculated in Swiss PDB Viewer 4.1 as determined by both distance and angle. The calculated hydrogen bond between the carbonyl of G358 and R756 is near the maximal distance, so its dashed line is colored *gray*. In the Na^+ form, R756 makes a hydrogen bond with the carbonyl of Q825. The glutamine's carboxyamido group in turn can form a hydrogen bond with the guanidine of Arg3 of the β subunit. There are minor shifts in predicted hydrogen bonds among the three conformations, but the common feature is that the guanidino group of R756 can make hydrogen bonds with three other parts of the protein that meet at this location. *D–E*, Na,K-ATPase (PDB file 3KDP) and a SERCA Ca-ATPase (PDB file 6LN5) were aligned on the cytoplasmic M5 helix with Magic Fit in Swiss PDB viewer to illustrate the interactions of R756 and R751. *F*, The two structures were superimposed. All of the bonded residues correspond between Na,K-ATPase and Ca-ATPase, and their relationships are exactly the same in the two proteins.

on the surface. Figure 1 shows that in the Na^+-bound conformation, one side of the guanidino group of R756 can form a hydrogen bond with the backbone carbonyl of an alanine (A599 in α3 numbering) in the second half of the P domain (P2) and the other side with a backbone carbonyl of a glutamine (Q825) on the cytoplasmic loop L6-7 between membrane spans M6 and M7. In two other conformations, there are only slight differences in the ground state: the alanine is farther away but is still within 4.2 Å, and in both ground state and the K^+-bound form, the hydrogen-bond to L6-7 is shifted to the carbonyls of R824 and I821. The carbonyl of a conserved glycine (G358 in ATP1A3) is also near the base of the guanidino group of R756, apparently within hydrogen bonding range; G358 is in the helix of the first part of the divided P domain, P1.

The result is a four-point contact of different parts of the protein anchored by the R756 guanidino group. In the homologous Ca^{2+}-ATPase SERCA2, the M5 arginine (R750), P1 glycine (G343), and P2 alanine (A616) are all conserved, as well as I815 and K818 in the L6-7 intracellular loop. Figure 1 (*right*) superimposes SERCA2 and Na,K-ATPase crystal structures to illustrate the similarity.

Our initial investigations in cell lines stably transfected with human ATP1A3 R756H determined that there was significant residual ATPase activity during growth at 37 °C. The principal questions were whether the activity is altered functionally; whether protein misfolding during biosynthesis contributes to pathogenicity; and whether the mutated protein is intrinsically temperature sensitive.

Results

Protein expression

The first objective was to assess the level of expression of ATP1A3 mutations in culture. Cell lysates were employed to ensure that all fractions, intracellular as well as plasma membrane, were included. Figure 2*A* shows a representative example of variations in ATP1A3 (α3) expression for several mutations in 293 isogenic cell lines after continuous tetracycline induction. D366H is an RDP mutation with an

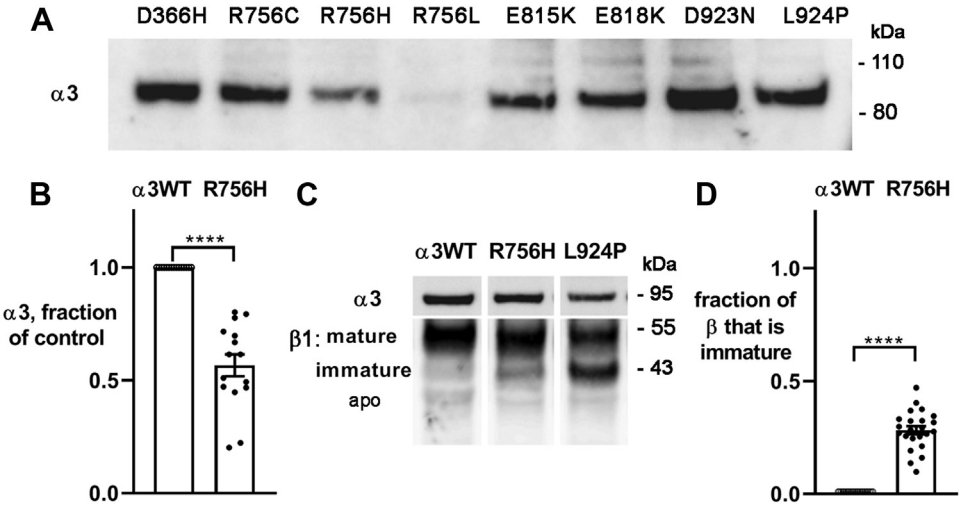

Figure 2. Reduced expression and increased ER retention. *A*, examples of variations in the expression level of α3 in 293 cell lines with different mutations. The R756L cells initially expressed the protein but looked abnormal and lost expression after continuous induction, suggesting selection against it. *B*, average reduction of R756H expression in 15 biological replicates, normalized to cells expressing WT α3 in the same experiment. Significance was determined with paired 2-tail Student's *t* test with the measured densitometry values for both α3WT and R756H (average 0.566 ± 0.188 S.D., n = 15, $p <$ 0.0001). *C*, example of differences in α3 expression and β subunit maturation. In almost all experiments with α3WT, immature β could not be quantified. This blot shows the highest level ever seen. All lanes shown were from the same blot, but top and bottom halves were stained with α3 and β1 antibodies separately, and unrelated lanes between these were removed. *D*, the fraction of immature β was determined by scanning densitometry of each lane for 23 independent samples from 15 experiments. Normalization for loading is not needed with in-lane scanning. Significance was determined by unpaired one-sided Student's *t* test (average 0.282 ± 0.086 S.D., n = 23, $p <$ 0.0001). Significance: ****≤ 0.00001.

inactivating substitution at the active site aspartate, and its expression level was consistently like WT (not included on this blot). R756C, R756H, and R756L are the three human substitutions that produce the relapsing encephalopathy and cerebellar ataxia (RECA)/fever-induced paroxysmal weakness and encephalopathy (FIPWE) syndrome. Each showed a different level of reduction of expression. The remaining lanes are E815K (a severe AHC mutation), E818K (CAPOS, cerebellar atrophy, areflexia, pes cavus, optic nerve atrophy, and sensorineural hearing loss), D923N (RDP), and L924P (EIEE). R756H was selected for investigation here because it is the most common RECA/FIPWE mutation. In multiple experiments its average expression, normalized to GAPDH, was reduced by about half relative to α3WT (Fig. 2*B*).

The first way that an amino acid substitution can damage a protein is by reducing its ability to fold during biosynthesis. Membrane proteins are folded in the endoplasmic reticulum (ER). When there is misfolding during biosynthesis, Na,K-ATPase α subunit with its β subunit is retained in the ER for additional rounds of chaperone-assisted folding. We previously reported that *ATP1A3* mutations D923N, L924P, and D742Y exhibited partial ER retention (1, 3). The migration of the Na,K-ATPase β subunit on SDS gels is an indicator: β subunit complexes with α subunit co-translationally (7, 8), and it is β that carries N-linked glycosylation. ER enzymes monitor the success of folding by successively trimming and rebuilding glucoses in the high-mannose glycoconjugate (9). All of the glycosylation in ER is in the high-mannose immature form, and β with immature glycosylation migrates faster than with mature glycosylation on SDS gels (8). Figure 2*C* shows that there is immature β in R756H cells, but not as much as in L924P cells in the same experiment. The proportion of the immature form for R756H was quantified by densitometry, and 25 to 30% of the β was retained (Fig. 2*D*). It should be borne in mind that β subunit also binds to the endogenous α1 subunit and traffics to the plasma membrane with it, so this is an underestimate of α3 misfolding.

Functional impairment by R756 mutations

Ouabain is a specific inhibitor of Na,K-ATPase. To make it possible to test the function of the inducible α3 separately from the endogenous α1 Na,K-ATPase, the human ATP1A3 cDNA in the vectors used to establish the cell lines had two amino acid substitutions that replicate the low ouabain affinity characteristic of rats and mice, while the endogenous human or monkey α1 expressed by the cells has high affinity (10). We performed the classic survival assay, where a low concentration of ouabain is used to inhibit endogenous α1 to determine if the induced α3 has enough activity to support cell growth. In both 293 and COS-1 cells, only R756H was able to survive in the presence of ouabain whereas R756C and R756L lines were unable to survive (see more in Methods). In COS-1 cells, the R756H line was maintained under ouabain selection. The ability of R756H to support cell survival in both HEK293 and COS-1 indicates that it has at least a minimum amount of pump activity that is successfully delivered to the plasma membrane.

Functional tests for enzyme expression and impairment were performed with membrane preparations from the stable R756H transfectants of COS-1 cells (Fig. 3). Following ouabain selection to obtain stable transfectants, an expression level 55% of WT was obtained by measuring the active site concentration in phosphorylation experiments determining the incorporation of ^{32}P from ATP under stoichiometric conditions (11)

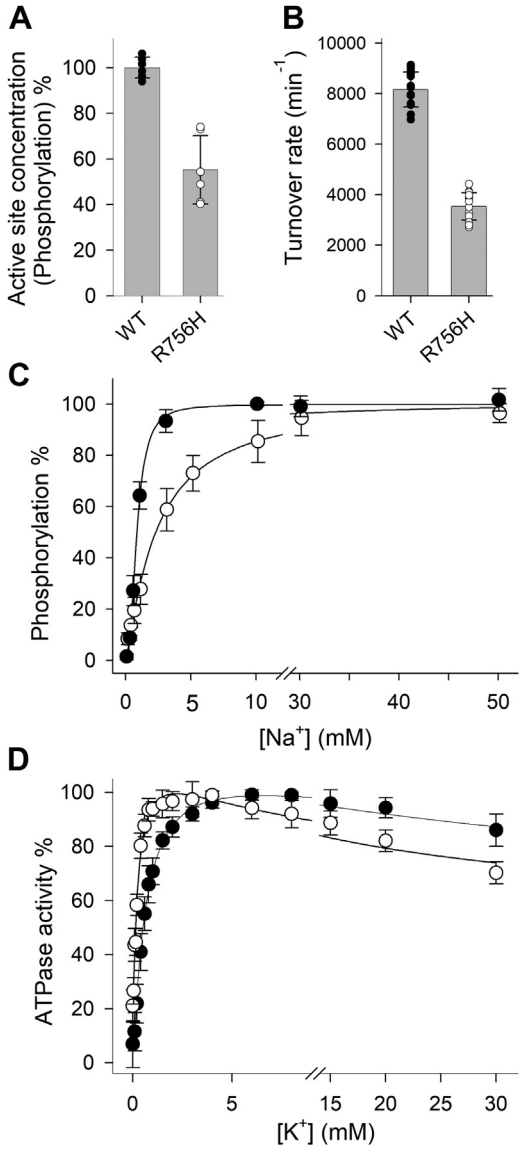

Figure 3. Impacts of the R756H mutation on Na,K-ATPase function. *A*, active site concentration as a measure of the expression level determined by phosphorylating the enzyme for 10 s at 0 °C in the presence of 2 μM [γ-^{32}P]ATP, 150 mM NaCl, 20 mM Tris (pH 7.5), 3 mM $MgCl_2$, 1 mM EGTA, 10 μM ouabain, and 20 μg oligomycin/ml, *i.e.*, under stoichiometric conditions (11). The data are presented as % of the WT, resulting in a mean value of 55 ± 15 (S.D., n = 6) for R756H. *B*, maximal catalytic turnover rate. The ATPase activity was determined for 15 min at 37 °C in medium containing 130 mM NaCl, 20 mM KCl, 30 mM histidine (pH 7.4), 1 mM EGTA, 3 mM $MgCl_2$, 3 mM ATP, and 10 μM ouabain and is shown relative to the active site concentration determined as described for panel A, resulting in mean values (min^{-1}) of 8157 ± 689 (S.D., n = 14) and 3531 ± 545 (S.D., n = 16) for WT and R756H, respectively. In panels A and B, the data points from individual determinations are shown superimposed on *bar graphs* showing mean values with *error bars* indicating S.D. *C*, Na^+ dependence of phosphorylation. Phosphorylation was carried out under conditions described for A, except that the Na^+ concentration was varied, added as NaCl with various concentration of $NMDG^+$ to maintain constant ionic strength. The data points (normalized to maximal phosphorylation) show mean values with error bars indicating S.D. Line plots represent the best fit of a Hill function. The apparent affinities for Na^+ activation extracted from the data are as follows: $K_{0.5}$ = 0.86 ± 0.04 mM and 2.56 ± 0.70 mM for WT and R756H, respectively (mean ± S.D., n = 3 and 6). *D*, K^+ dependence of Na,K-ATPase activity determined at 37 °C in medium containing 40 mM NaCl, 3 mM ATP, 3 mM $MgCl_2$, 30 mM histidine (pH 7.4), 1 mM EGTA, 10 μM ouabain, and the indicated concentrations of K^+ added as KCl. The data points (normalized to the maximal activity) show mean values with error bars indicating S.D. Line plots represent the best fit of a double Hill function to the data (with a rising phase and an inhibition phase). The apparent affinities for K^+ activation extracted from the data corresponding to the rising phase are: $K_{0.5}$ = 595 ± 66 μM and 213 ± 25 μM for WT and R756H, respectively (mean ± S.D., n = 5 and 6).

(Fig. 3*A*). To eliminate expression level and possible inactivation in the cell culture as variables, the maximal catalytic turnover rate was determined by relating the rate of ATP hydrolysis by the isolated membrane preparation to the measured concentration of active sites in the same preparation. As shown in Figure 3*B*, the maximal turnover rate of R756H, determined in the presence of saturating Na^+ (130 mM) and K^+ (20 mM), was approximately half of that of WT in the same conditions. Figure 3*C* shows that the apparent affinity for Na^+ required for the *in vitro* incorporation of phosphate from ATP and Mg^{2+}, as determined in the absence of competing K^+ and in the presence of oligomycin to block dephosphorylation, was reduced approximately 3-fold compared to WT. Figure 3*D* shows that the apparent affinity for K^+, measured by its activation of ATP hydrolysis in the ATPase assay with Na^+ present to activate the active site phosphorylation, was higher in R756H than in WT, with half-maximal stimulation at ∼200 μM compared to 600 μM in WT. A reduced apparent affinity for Na^+ has been seen in a number of pathogenic human Na,K-ATPase mutants (12). Because the Na^+ concentration in cells is not saturating for the cytoplasmic-facing Na^+ sites, a reduction in apparent Na^+ affinity is expected to reduce physiological activity (activity at the cytoplasmic concentration of Na^+) in addition to the reduced turnover number and reduced expression level (11). While the activation of phosphorylation is due to Na^+ binding at the sites facing the cytoplasm in intact cells, the K^+ activation of the ATPase activity owes to K^+ binding at the sites facing the external side of intact cells. The K^+ dependence of ATPase activity (Fig. 3*D*) furthermore reveals an inhibition of ATPase activity at high K^+ concentrations that can be ascribed to competition between Na^+ and K^+ at the internal sites where Na^+ activates. This inhibition is more pronounced in R756H relative to WT, likely due to the reduced Na^+ affinity at these sites. Hence, the E1-E2 conformational equilibrium is likely displaced toward E2 in the mutant. The increased apparent affinity for K^+ in activation of ATPase activity may likewise result from enhanced competition of K^+ with Na^+, but in this case at the extracellular-facing sites, where K^+ exerts its activation of dephosphorylation.

Temperature sensitivity

Given that ATP1A3 R756 symptoms begin during febrile infections, it is a cardinal question whether R756H is intrinsically temperature sensitive. We tested whether elevation of temperature in the febrile range (to a conservative 39 °C) elicits a heat shock response in 293 cells. The cytoplasmic chaperone HSP70 was elevated ∼2-fold over baseline when both α3WT and R756H 293 cultures were shifted to 39 °C for 24 h (α3WT, average 2.02 ± 0.27 SD; R756H, average 2.11 ± 0.38 SD. p = 0.0005 for α3WT and p = 0.001 for R756H

by one-tailed *t* test, N = 5). This indicates that there is a robust protective heat shock response in these conditions.

The expression of Na,K-ATPase subunits during the same temperature elevation protocol is shown in Figure 4*A*. The α3 in α3WT and R756H lines was continuously tetracycline-induced, and the α1 and β1 were endogenous. Expression of R756H α3, which was already reduced at 37 °C (Fig. 2*B*), was further reduced at 39 °C (Fig. 4, *A* and quantification in *B*). The average final level of α3 expression was estimated by multiplying R756H expression at 37 °C (65% that of α3WT) by the level at 39 °C (47%) to give a final average level of 31% (n = 9 matched biological replicates).

The expression of endogenous α1 is not independent of the expression of α3 in this system (1, 3). Reciprocal expression of the two α isoforms was seen when 293 cells are cultured continuously in tetracycline, which suggests that they compete for a factor that physiologically limits the total. This is consistent with prior reports in other types of cells (8, 13, 14), although the mechanism is still not known. In elevated temperature experiments here, any increase in α1 for α3WT-expressing cells was not statistically significant, but in R756H cells, α1 had a significant ∼50% increase at 39 °C (Fig. 4*C*) corresponding to the ∼50% decrease in α3 (Fig. 4*B*). There was no change in the total β subunit detected in α3WT or R756H cells after incubation at 39 °C for 24 h (Fig. 4*D*). The ratio of β to α3 was elevated 2-fold in R756H at 39 °C, corresponding to the reduction in α3.

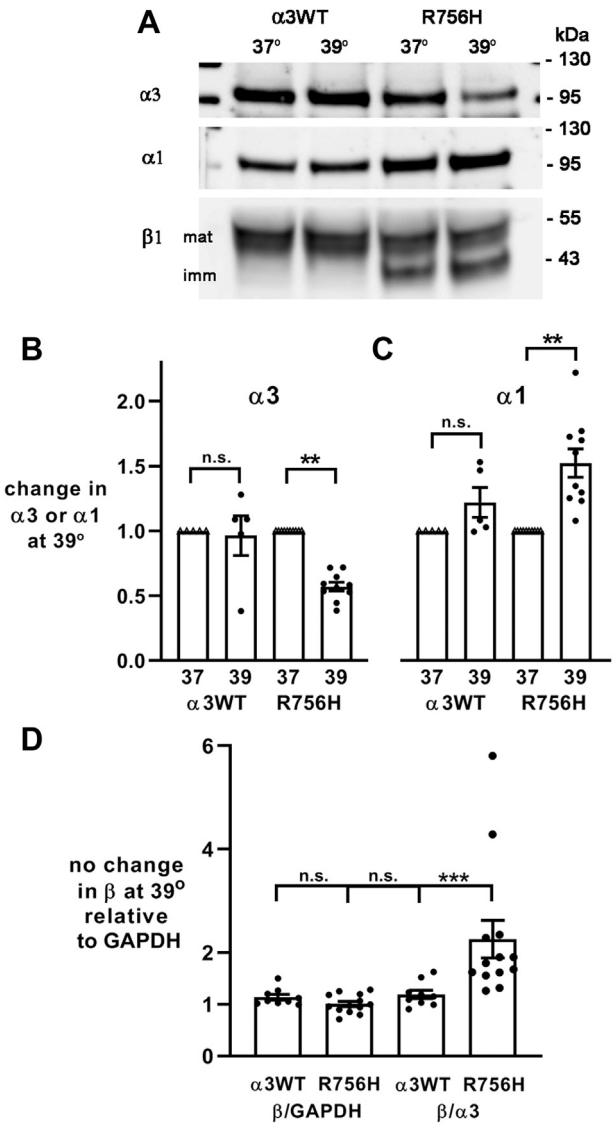

Figure 4. Elevated temperature effects on Na,K-ATPase α and β subunits. *A*, the blots shown are from the same experiment as Figure 3*A*. *B* and *C*, α3 and α1 were quantified by densitometry. There was little effect of elevated temperature on α3WT, but there was complementary reduction in α3 and increase in α1 in R756H. Biological replicates were n = 5 for α3WT (α3 average 0.963 ± 0.343 S.D.; α1 1.104 ± 0.416 S.D.) and n = 10 for R756H (α3 average 0.571 ± 0.106 S.D.; α1 1.522 ± 0.344 S.D.). Statistical analysis was by Wilcoxon-signed rank test ($p < 0.01$). *D*, total β subunit was quantified by densitometry and normalized to GAPDH (*left* 2 bars), and there was no significant difference by paired 2-tail Student's *t* test (α3WT average 1.139 ± 0.164 S.D, n = 9; R756H 1.018 ± 0.200 S.D, n = 9). On the *right*, when total β subunit was normalized to α3 in each experiment, the difference was significant ($p <$ 0.001), reflecting the decrease in α3 (α3WT average 1.194 ± 0.239 S.D, n = 9; R756H 2.262 ± 1.394 S.D, n = 13). Significance: **≤0.001; ***≤0.0001.

Temperature-sensitivity in vitro

The temperature sensitivity of R756H compared to control α3WT was tested in controlled conditions *in vitro* using membrane preparations from stable COS-1 cell lines. The results are shown in Figure 5. Following incubation for various time intervals at 37 °C, 39 °C, or 41 °C, the ATPase activity was determined under standard conditions at 37 °C. The WT was rather stable, losing only about 20% of the activity during 24 h incubation in the presence of 130 mM Na^+ and 20 mM K^+ (*i.e.*, saturating concentrations), with little effect of the

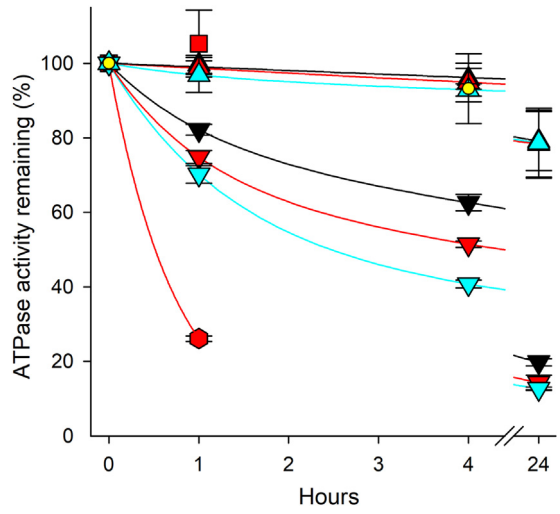

Figure 5. Temperature sensitivity *in vitro*. Wildtype (*triangles pointing upward*), R756H mutant (*triangles pointing downward*), and D923N mutant (*small yellow circles*) in membranes isolated from COS-1 cells and permeabilized as described in Methods were incubated for the time intervals indicated on the abscissa in buffer containing 12.5 mM Imidazole (pH 7.0), 10 mM EDTA, with 130 mM NaCl and 20 mM KCl, at the following temperatures: 37 °C (*black symbols*), 39 °C (*red and yellow symbols*), or 41 °C (*cyan symbols*). At the indicated times, the ATPase activity was determined. Mean values are shown relative to that corresponding to zero time. Plotted on the same graph (*red squares*, WT; *red hexagons*, R756H) are the values obtained when membranes were incubated at 39 °C in buffer containing 12.5 mM Imidazole (pH 7.0), 10 mM EDTA without NaCl or KCl, which destabilized the R756H mutant far more than WT. Error bars indicate S.D. (number of independent experiments n= 3–6 for all datapoints, each performed as duplicate determinations).

temperature differences. By contrast, under similar conditions the R756H mutant lost more than 80% of activity with a noticeable temperature dependence of the inactivation rate, which was 20- to 30-fold higher than that of WT, as estimated from the decay during the first hour of incubation at the various temperatures. In the absence of added Na^+ and K^+, the WT remained as stable as in the presence of 130 mM Na^+ and 20 mM K^+, but the inactivation rate of the mutant increased further to more than 100-fold that of WT (Fig. 5). The stability of WT demonstrates that the effect of removing Na^+ and K^+ from the mutant is not a simple consequence of low ionic strength or absence of the physiological ligands; a particular structural instability caused by the mutation seems to be required. These results prompted us to examine another neurological disease mutant, α3-D923N causing RDP/AHC, which previously was shown to exhibit very low affinity for Na^+ (in fact more than 100-fold reduction relative to WT) (15). As can be seen in Figure 5 (yellow circles), this mutant was as stable as WT at 39 °C, again showing that the instability of R756H is a unique property of its protein structure and not due to reduced Na^+ binding.

Recovery from elevated temperature

Patient phenotype includes gradual recovery (>1 month) of much normal function after a febrile illness subsides. We tested whether expression of α3 in R756H 293 cells recovers if cells are returned to normal temperature. For these experiments, incubation at 39 °C was extended to 48 h, with new controls. Figure 6, *A* and *B* show that the temperature-induced reduction of α3 in R756H cells was essentially the same at 24 h and 48 h. Figure 6*C* shows a secondary phenomenon that there was a modest improvement in the maturation of the R756H β subunit when incubation at 37 °C was extended to 48 h. This may be due to accumulation of the mature glycosylated form because the plasma membrane area increases as cell processes gradually lengthen after trypsinization. This is also seen in the maturation of β at elevated temperature at the same time points, as shown in Figure 6*D*. After incubation at 39 °C for 24 h, the fraction of immature β was modestly higher at 39 °C than at 37 °C in R756H cells, and the difference between 37 °C and 39 °C was statistically more significant at 48 h ($p < 0.001$). These are small effects on β, but they could play a larger role in cells that do not proliferate, like neurons. The total amount of β was unchanged after 48 h of elevated temperature (Fig. 4*D*). Considered together, the unaltered total β and minor effect on its maturation contrast with the sharp reduction of α3 in R756H cells.

To test for recovery, α3WT and R756H cultures were incubated at 37 °C or 39 °C for 48 h and in parallel at 39 °C for 24 h followed by 24 h at 37 °C (Fig. 7*A*). This resulted in substantially restored expression of R756H α3 normalized to

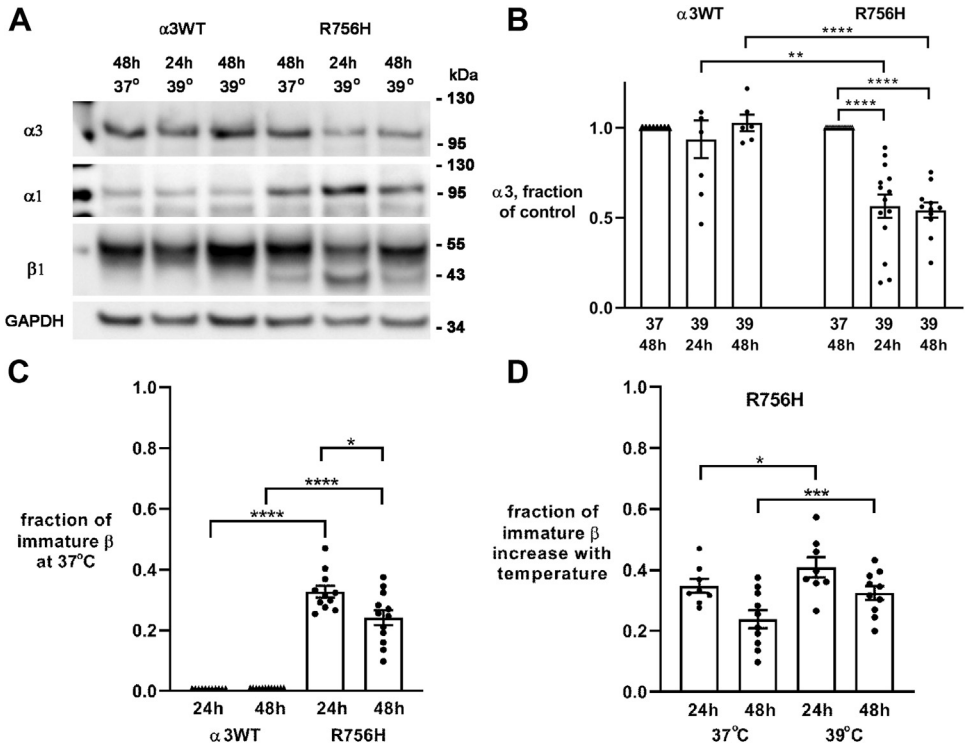

Figure 6. Prolonged incubation of cells at elevated temperature. *A*, representative Western blot showing the effect of prolonging incubation at 39 °C to 48 h. The *asterisk* in panel A marks immature β. *B*, α3 levels remained suppressed at 48 h; by two-way ANOVA, levels in α3WT were not different (average 0.936 ± 0.296 S.D. at 24 h, n = 8; 1.027 ± 0.112 S.D. at 48 h, n = 6; n.s.) and R756H was reduced by half ($p < 0.01$) (average 0.567 ± 0.243 at 24 h, n = 14; 0.543 ± 0.139 S.D. at 48 h, n = 11). The figure additionally shows pairwise 2-tailed comparisons. *C*, effects of the length of incubation on the fraction of β subunit that is immature were quantified at 37 °C to determine the baseline, and the graph shows 24 h and 48 h data (average 0.327 ± 0.065 S.D. at 24 h, n = 11; 0.241 ± 0.085 S.D. at 48 h, n = 12). Improved maturation at 48 h for R756H cells was significant at 37 °C ($p < 0.01$). *D*, the proportion of immature β subunit in R756H was higher at 39 °C at both incubation times, but the difference was greater after 48 h. Two-way ANOVA gave $p < 0.01$, and a pairwise 2-tailed *t* test between 37 °C and 39 °C were more significantly different at 48 h ($p < 0.001$). Averages were 37 °C 24 h 0.348 ± 0.064 S.D, n = 8.; 37 °C 48 h 0.266 ± 0.081 S.D. n = 8; 39 °C 24 h 0.409 ± 0.95 S.D. n = 8; 39 °C 48 h 0.324 ± 0.072 S.D., n = 10). Significance: *≤0.01; **≤0.001; ***≤0.0001; ****≤ 0.00001.

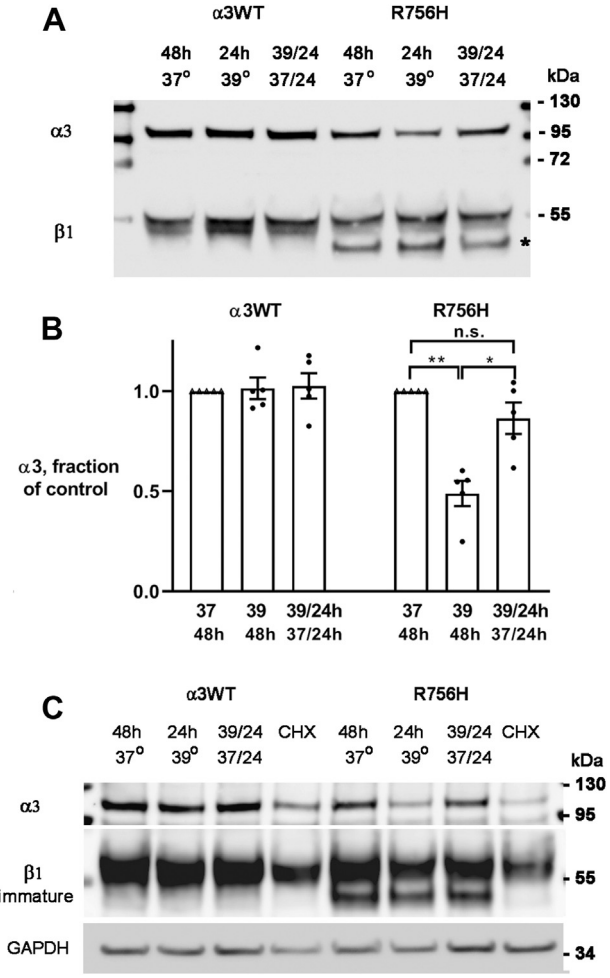

Figure 7. Recovery after elevated temperature. *A*, representative blot showing recovery of α3 expression after shift from 39 °C back to 37 °C. *B*, the averaged data showed no significant change in α3WT expression levels (n = 5) (average 1.015 ± 0.120 S.D. at 37 °C, 1.028 ± 0.142 S.D. at 39 °C), but for R756H, the data were significant by two-way ANOVA and pairwise comparisons (n = 5) (average 0.489 ± 0.140 S.D. at 37 °C, 0.866 ± 0.175 S.D at 39 °C). Significance: *≤ 0.01; **≤0.001. *C*, cycloheximide blocked the recovery of R756H α3 as expected if most of the recovery is due to new synthesis. The reduction in α3WT due to cycloheximide was 25% for α3 and undetectable for total β, while for R756H, the reduction was 65% for α3 and 25% for total β.

GAPDH (Fig. 7*B*). When cycloheximide was added to block new protein synthesis at 24 h with the shift to 37 °C, the recovery of α3 was 25% lower in α3WT but was 65% lower in R756H (Fig. 7*C*). This indicates both that the recovery of R756H is largely due to new protein biosynthesis and that mature R756H α3 is degraded more quickly. During recovery experiments, no consistent difference in the proportion of immature β subunit was detected 48 h at 39 °C, n = 12, average 0.218 ± 0.66 SD; 24 h 39 °C, 24 h 37 °C, n = 4, average 0.320 ± 0.053, p = 0.383). Panel C shows that immature β subunit disappeared during cycloheximide treatment, however, suggesting that it completed its maturation in the Golgi apparatus or was degraded during the chase.

Phenylbutyric acid

L924P is an *ATP1A3* mutation with severe consequences at infancy and was studied previously (1). Treatment of 293 cells expressing L924P with the folding drug and histone deacetylase inhibitor phenylbutyric acid (PBA) improved the accumulation of the L924P α3 mutant and the maturation of the β subunit (3). The same treatment was tested here for R756H. Figure 8 shows that PBA had only slight benefits for either the amount of mutant α3 or the maturation of β glycosylation (Fig. 8, *A* and *B*) and none at 39 °C.

The effect of PBA on the L924P mutation had a functional readout; there was a 40% reduction in the median length of cell processes in L924P cells growing on tissue culture plastic compared to α3WT, and this was corrected by PBA treatment (3). Process length in cells expressing R756H was not affected by the mutation even after incubation for 48 h at 39 °C (Fig. 8, *C* and *D*). The L924P mutation had a much bigger effect on β subunit ER retention than R756H, indicative of a strong UPR that may have diverted resources from process extension. That was evidently not a major factor for R756H. This is the kind of difference in mutation impact on cell behavior unrelated to ion transport that may underlie phenotype diversity among ATP1A3 mutations.

Immunofluorescence detection of R756H

HEK293 cells mound up when crowded, which gives the opportunity to visualize normal cell–cell interactions mediated by the transassociation of Na,K-ATPase β subunits between neighboring cells (16, 17). This gives the anti-β fluorescence the appearance of brighter, straighter lines at cell interfaces. The ATP1A3 mutation L924P showed profound disruption of this interaction and rounded, variable-sized cells (1). Here, cultures were fixed at a density where most cells were in contact as monolayers or mounds where such features can be observed with conventional fluorescence microscopy.

Figure 9*A* shows Na,K-ATPase stain after growth at 37 °C. Cells expressing α3WT had the classic honeycomb appearance of crowded cells somewhat flatly apposed to each other (Fig. 9, *A*, *A–C*). As expected for dividing cells, there was always some intracellular stain, but colocalization of α3 and β1 was good. In contrast, cells expressing R756H had disrupted localization (Fig. 9, *A*, and *D–F*). A majority of α3 stain appeared to be intracellular, with occasional aggregates. β subunit localization was variably disrupted and showed a mixture of membrane and intracellular distribution.

After incubation at 39 °C for 24 h, the α3WT control cells showed more intracellular stain, but colocalization of α3 and β1 was unchanged (Fig. 9, *A–C*). R756H cells were more sensitive to elevated temperature. At least two kinds of pathology were seen. Some cells were larger, and less α3 stain could be seen at cell margins. These R756H-expressing cells had faint and diffuse aggregates in the cytoplasm (Fig. 9, *B*, and *D–F*). In this case, β subunit appeared to colocalize in the internal fraction. Other cells showed less internalization and better colocalization with β subunit, and there were occasional cells with very abundant and bright internal aggregates (Fig. 9,

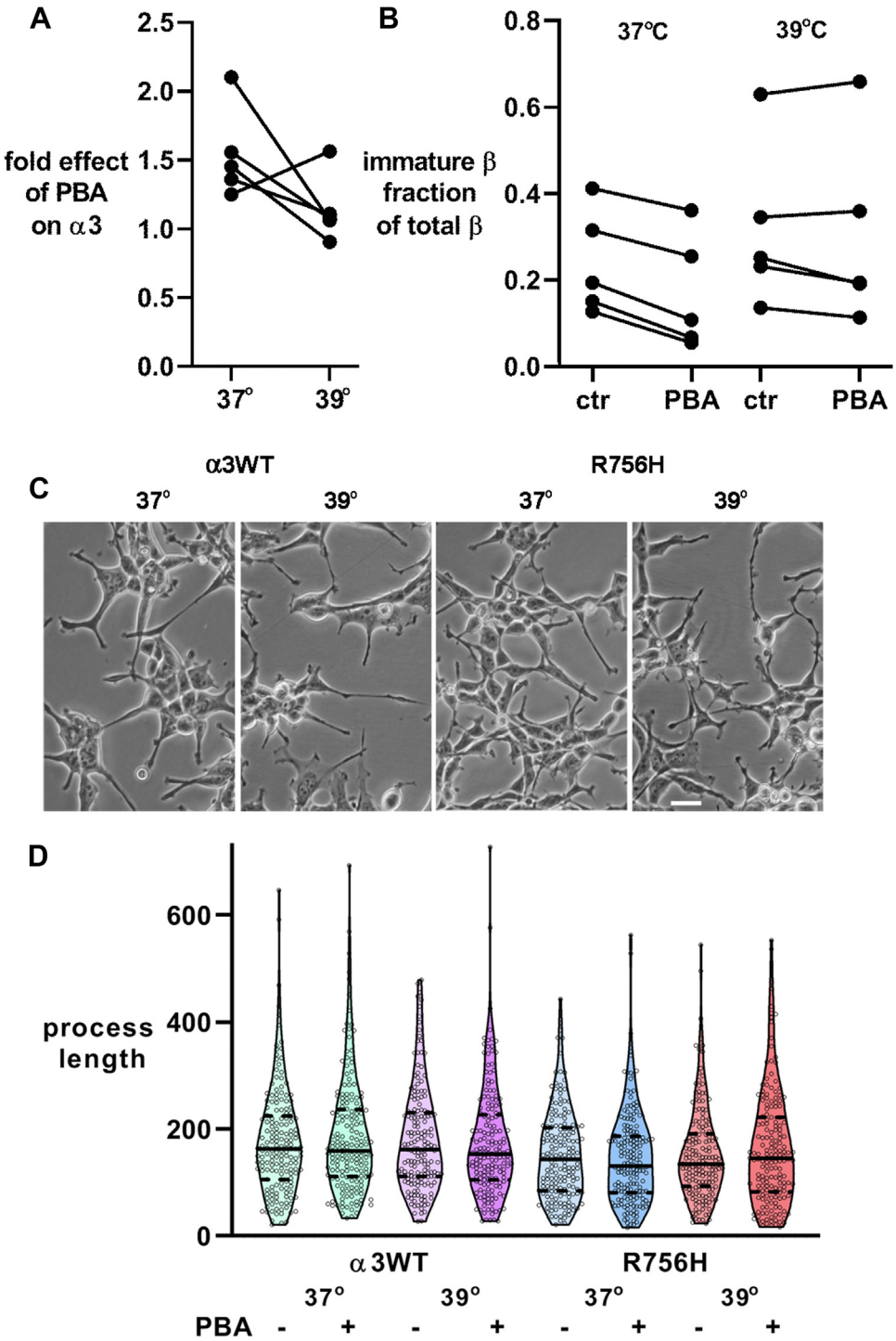

Figure 8. Tests of phenylbutyric acid (PBA) for improvement of R756H cell phenotype. *A*, R756H cells were incubated at 37 °C or 39 °C for 48 h with and without 5 mM PBA. At 37 °C, there was an average 1.48-fold increase in α3 in R756H, but this did not differ from 1.46-fold in α3WT. At 39 °C, there was less improvement than at 37 °C. *B*, similarly, there was a small improvement in β maturation in PBA at 37 °C, but not at 39 °C. The results are plotted as pairs of values in five replicate experiments. *C*, the appearance of processes was not different between α3WT and R756H at either temperature. Scale bar is 20 μm. *D*, quantification of process length (175 measurements per condition) showed that α3WT and R756H had a similar distribution of lengths at both temperatures and with and without PBA.

B, and *G–I*). In the latter case, α3 formed aggregates with a broad cytoplasmic distribution. In such clusters of cells, there was very little colocalization of α3 with β. The pathology was thus heterogeneous, suggesting the activation of different kinds of deleterious responses.

Involvement of lysosomes

Antibody to lysosomal-associated membrane protein 1 (LAMP1) was used as a marker of lysosome and late endosome morphology, while antibody to β1 gave definition to cell boundaries (Fig. 10). At 37 °C, there was little difference in the

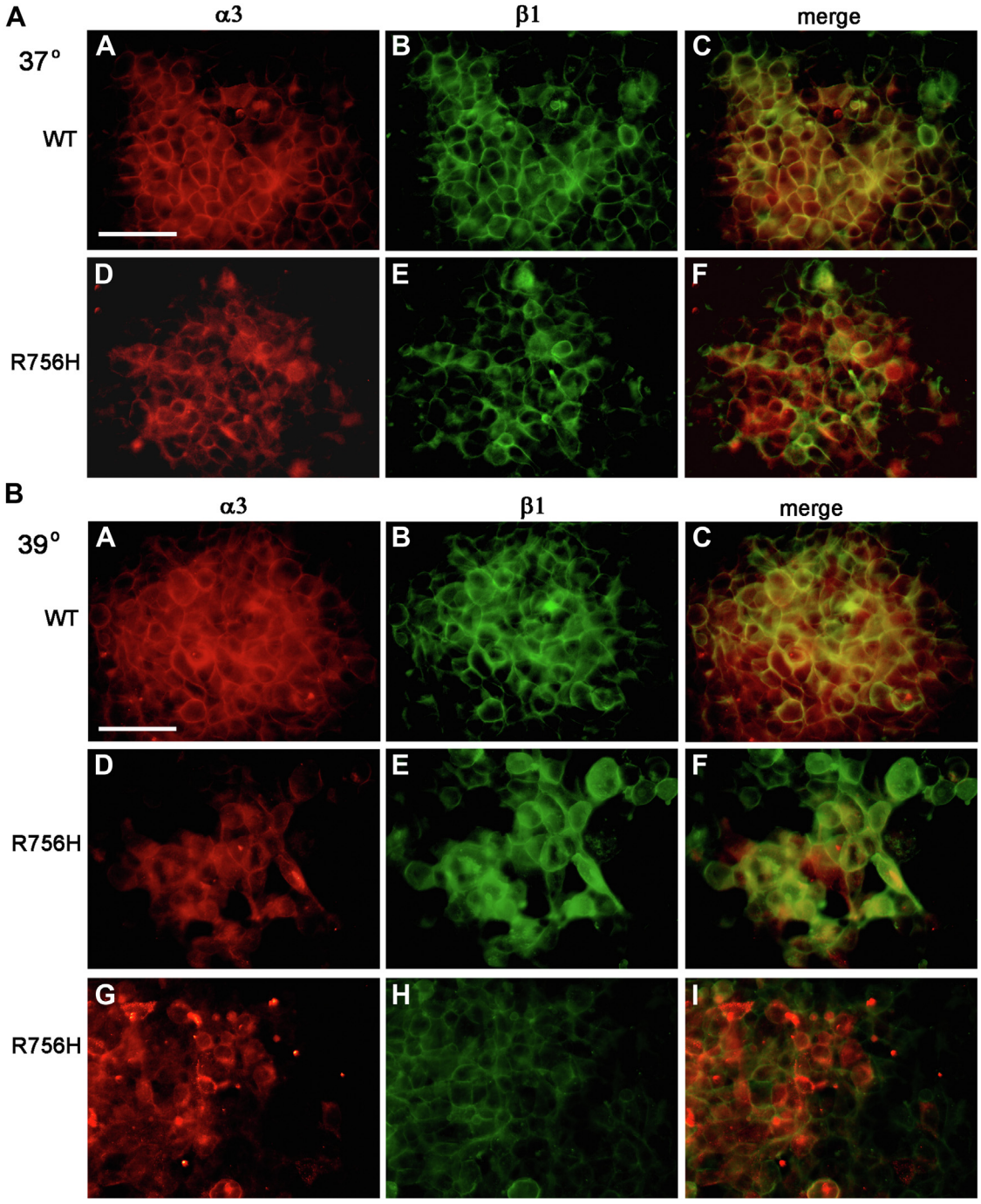

Figure 9. α3 and β1 distribution in confluent cells. In fixed and permeabilized cells, α3 was detected with polyclonal antibody (*red*) and β1 with monoclonal antibody M17-P5-F11 (*green*). *A*, after growth at 37 °C, R756H cells showed more intracellular stain and more discrepancies in the distribution of α3 and β compared to the α3WT controls. *B*, after growth at 39 °C, α3WT showed uniform changes consisting of an increase in intracellular stain. R756H cells, on the other hand, showed almost entirely intracellular stain for α3 as well as cells with sharply reduced levels. The β subunit in many cases was internalized, but with less co-localization with α3. *D–F*, these images show cells that are somewhat enlarged, with diffuse stain. *G–I*, these cells show a different pathology consisting of bright α3 aggregates scattered in the cytoplasm. Scale bar 50 μm.

appearance and distribution of LAMP1 stain between α3WT and R756H cells. After incubation at 39 °C, there was considerable increase and dispersion of LAMP1 stain in R756H cells. This appears to parallel the internalization and loss of stain for α3. Chloroquine (CQ) blocks the fusion both of autophagosomes activated by the accumulation of aggregated protein and intermediate vesicles originating from internalization of damaged protein from the plasma membrane (18). CQ treatment at the same time as 39 °C incubation blocked the anatomical effect on LAMP1. However, CQ did not significantly block the reduction of R756H levels detected on western blots either at control temperature or at 39 °C (α3WT: average 1.047 ± 0.153 SD at 37 °C; 1070 ± 0.300 at 39 °C. R756H: 1.298 ± 0.325 at 37 °C; 1.451 ± 0.525 at 39 °C,

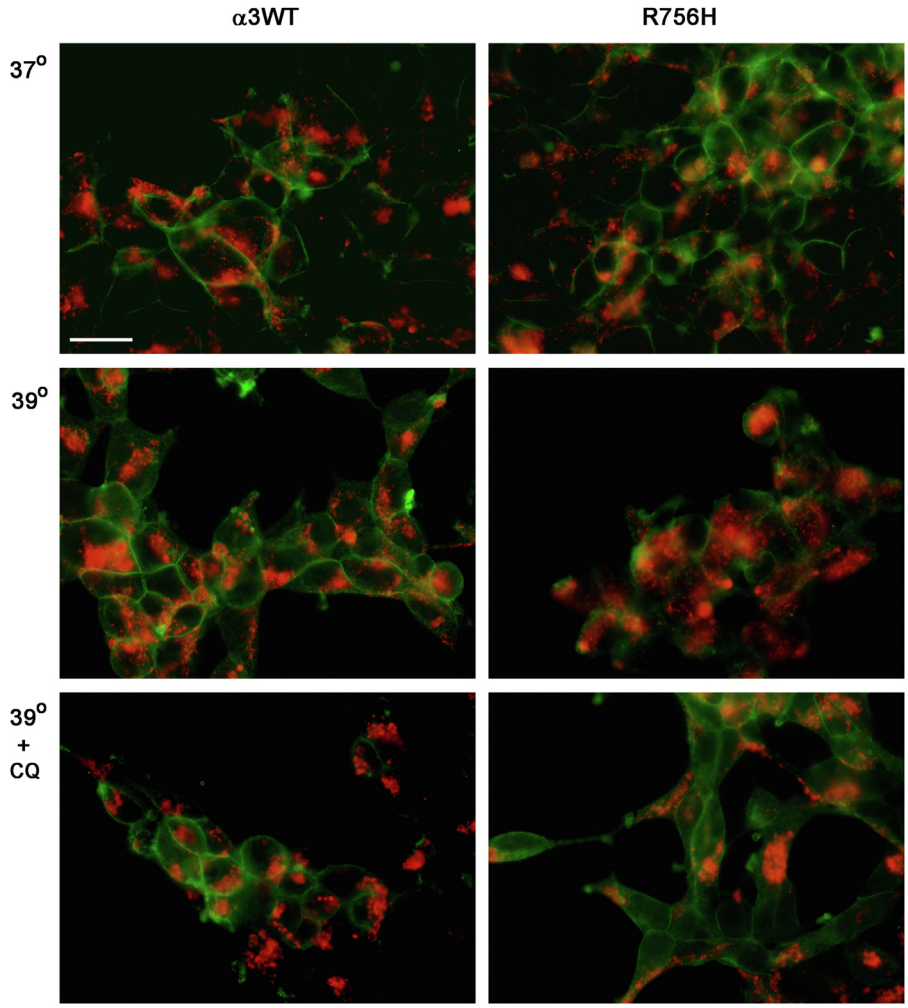

Figure 10. LAMP1 stain for lysosomes and endosomes. Stain for LAMP1 is *red*, and stain for Na,K-ATPase β subunit in *green* is used to define the edges of the cells and reveal some disruption in R756H cells. Chloroquine, 10 μM, was added at the same time as the change to 39 °C. Scale bar 20 μm. LAMP1, lysosomal-associated membrane protein 1.

n = 3. T-tests: effect of temperature on CQ, 0.91 for α3WT, 0.70 for R756H.; effect of mutation, 0.29 at 37 °C, 0.23 at 39 °C). It seems likely that two things are occurring; mature Na,K-ATPase in the plasma membrane is damaged and routed to lysosomes, while ongoing biosynthesis of R756H is compromised by elevated temperature. Heat shock induces major changes in physiology, and so understanding how the damaged R756H enzyme is degraded under the stress of fever will require more investigation.

Prediction of the impact of R756 mutation

As shown in Figure 1, R756 is a highly conserved residue with a core role in P-type ATPase structure. Hydrogen bond stabilization of a point where multiple contacts form between linearly distant segments has implicit significance, particularly given that the contacts are with backbone, not side chains. Figure 11 shows what interactions are missing and what are possible (without adjustments during folding) in the three R756 mutants. When histidine is substituted for arginine in the crystal structure, three out of six rotamers clash with the carbonyl of G358, and the other three clash with the side chain of I821. When cysteine is substituted, one of three rotamers produces a hydrogen bond between the sulfur group and the carbonyl of G358, as also noted in a recent case report (19), and the other two rotamers do not clash. When leucine is substituted, one of four rotamers clashes with the carbonyl of V752, which also normally forms a backbone α-helical hydrogen bond with it. A different rotamer clashes with the side chain of I821, while the other two rotamers of leucine do not clash.

Discussion

Phenotype-genotype relations

This investigation adds another piece to the puzzle of phenotype variability in human mutations of the *ATP1A3* gene. The most extensively studied differences between mutation properties investigated in mammalian cells, insect cells, or oocytes are different extents of activity loss, different kinetic constants for Na^+, K^+, and ATP, and different voltage sensitivities. Here we show that R756H has reduced maximum activity, reduced apparent affinity for Na^+, and increased apparent

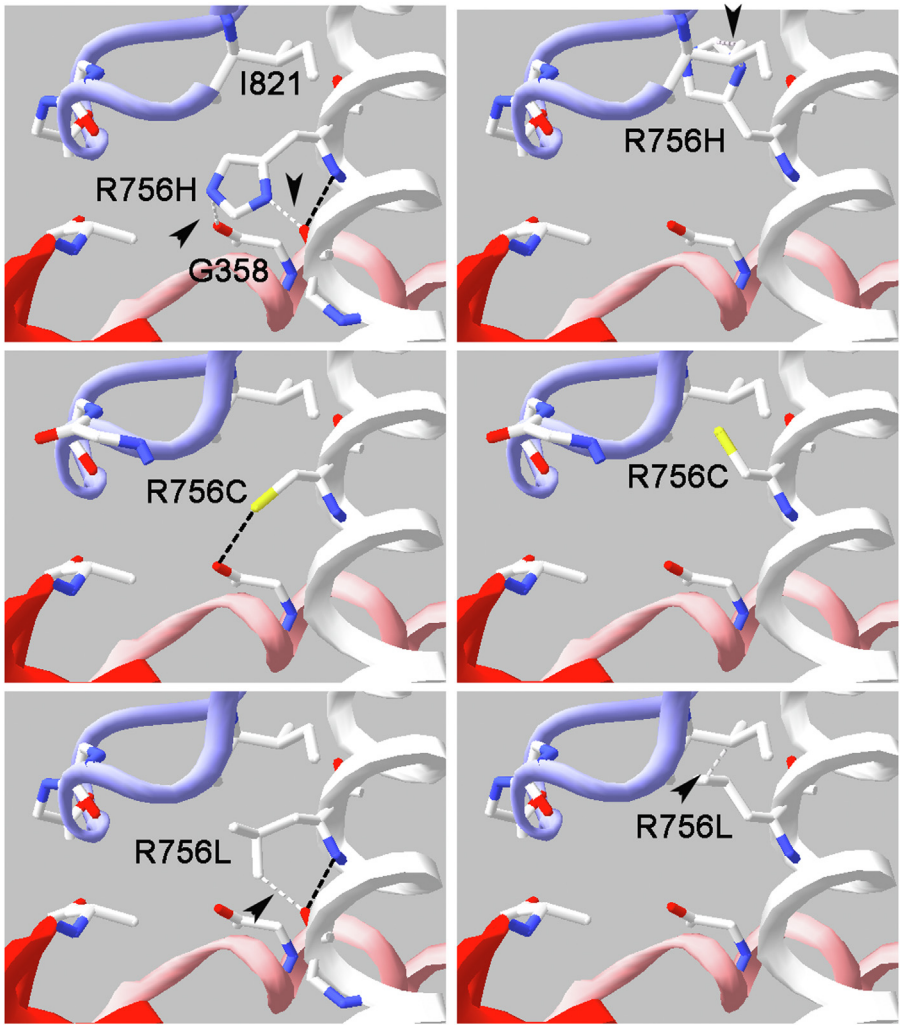

Figure 11. Rotamers predict interactions of the mutant side chains. Substitutions were made in the Na^+ form crystal structure 3WGU with the Swiss PDB viewer, and each of their rotamers was examined for interactions or clashes with other residues. Two examples are shown for each substitution to histidine, cysteine, and leucine. On the left in each frame, the backbone carbonyls and amides of A599 in the P domain and Q825 and R824 in L6-7 are shown to illustrate how far away the side chains of the three substitutions are. *Black dashed lines* are calculated hydrogen bonds. The bond that shows in both R756H and R756L is the normal alpha helical hydrogen bond between the carbonyl of V752 and the amide of R756. A new hydrogen bond is predicted between the sulfur of cysteine and the carbonyl of G358. Clashes are indicated by *white dashed lines* and by *arrowheads* when poorly visible.

affinity for K^+. The effects on Na^+ and K^+ interaction resemble several other Na,K-ATPase neurological disease mutations, particularly in ATP1A3 (11, 12, 15). It should be recognized that at the physiological intracellular Na^+ concentration in the presence of competing K^+, the reduction of Na^+ affinity may render the amount of Na^+-bound enzyme rate limiting for the overall transport reaction. The pump activity under physiological conditions would be further challenged by the reduced maximal turnover rate and reduced expression level of active enzyme. Although this would affect the intracellular concentrations of Na^+ and K^+ and as a result also the membrane potential and Ca^{2+} in neurons, there isn't yet an obvious correlation between functional differences and human phenotype. Hence, the disturbance of pump function would not explain the specific phenotype observed for R756H, which is characterized by fever-induced symptoms. There also isn't compelling evidence in favor of haploinsufficiency in the phenotypes we know about, though it remains formally possible.

Phenotype differences may instead arise from toxic side effects of mutation. Previously, we showed that protein misfolding and the UPR were exhibited by two mutations with severe manifestation in infancy or atrophy later, as well as activation of a proapoptotic pathway (1, 3). Here, the fever-induced symptoms seem to be explained by the *in vitro* observation of a temperature-dependent inactivation of the ATPase activity of R756H that is 20- to 30-fold faster than seen for WT. In the absence of the natural ligands Na^+ and K^+, the rate of inactivation of the R756H mutant was even higher, more than 100-fold increased relative to WT, thus indicating a dramatic destabilization of the protein structure. This destabilization is not due to the absence of physiological ligands as indicated by the high stability of WT in the absence of these ligands. Neither is it due to the reduced Na^+ affinity of R756H, because another ATP1A3 neurological disorder mutant D923N with more than 100-fold reduction in Na^+ affinity, due to perturbation of the third Na^+ binding site, did not show

instability relative to WT. This is well-explained by the role of the R756 guanidine group as a strategic anchor that promotes the interaction between key functional subdomains of the ATPase (P1, P2, L6-7 loop, and M5) by hydrogen bonds. Without the stability provided by the hydrogen bonds to R756, thermal energy input may allow the subdomains to escape their intimate contact and unfold. Furthermore, at elevated temperature, cells showed apparent internalization of R756H from the membrane, degradation, and after return to normal temperature, replacement with new protein as the principal way to recover. Such a scenario is in line with the clinical observations of recovery following the fever.

Figure 1 showed the particular role of the extended side-chain of R756 (or Arg750 in ATP2A1) of forming hydrogen bonds with the backbone carbonyls of residues in L67, P1, and P2. Figure 11 shows the lack of these bonds when the rotamers of His, Cys, and Leu are substituted in the existing protein structure. There would also be atom clashes with some rotamers. During protein folding, clashes can result in impaired or delayed success. When a protein does fold, clashes will result in adjustments in the position of surrounding residues. This is the basis of long-range effects on protein structure and function. Here, the degree of clashes differs among the substitutions, yet the fever-sensitive phenotype in patients is similar. This suggests that it is the absence of the guanidino group and its hydrogen bonds that confers temperature sensitivity in ATP1A3. With the Na,K-ATPase mutation tested here, expression was reduced, but sufficient material was produced for analysis of enzyme kinetics after growth at normal temperature. At 37 °C, there was a clear reduction in turnover number with reduced affinity for Na^+ and increased affinity for K^+, demonstrating long-range effects on structure and function; however, activity was lost at 39 °C.

In support of this interpretation, the corresponding arginine's sensitivity to mutation was first seen in laboratory attempts to mutagenize SERCA to investigate mechanism and kinetics (20). R751 was changed to alanine, isoleucine, or glutamate in ATP2A1, but the result was poor expression in COS cells. The conservative mutation R751K was tolerated and expressed well but had no ATPase activity. These findings were notable because 17 other mutations in the vicinity were expressed and had activity, and their effects on enzyme kinetics were documented in the same study.

Is fever a common precipitating factor in genetic disease?

There is evidence that Na,K-ATPase studied *in vitro* is not unusually sensitive to thermal inactivation (21, 22). On the other hand, there are many clinical case reports of responses to fever in people with other mutations not only in ATP1A3 but also in a wide range of other genes. There is another mutation-specific ATP1A3 syndrome, CAPOS, with the mutation p.Glu818Lys, that is triggered by febrile infections (23). Familial hemiplegic migraine patients with mutations in *ATP1A2*, the gene for the Na,K-ATPase expressed in glia in the brain, frequently have seizures, and in one paper seven out of 27 families reported febrile seizures (24). However, triggering by fever does not necessarily mean temperature sensitivity of the protein structure. Fever is a defensive strategy to fight infection or trauma, and it entails a metabolic cost and other costs in the form of tissue damage. Fever may be accompanied by stress, inflammation, immunomodulation, cytokine elevation, and cell death (25), phenomena that could alternatively trigger disease. It is not yet known whether thermal protein destabilization plays a role in any of the other known Na,K-ATPase mutation cases.

Homologous human mutations in other P-type ATPase genes

The residue corresponding to R756 is mutated in other diseases. In ATP1A2 (the Na,K-ATPase α2 subunit that is expressed in glia), R763H and R763C have both been reported in familial hemiplegic migraine (FHM2) (26–29), as has A606T, the residue corresponding to A599 in ATP1A3 (30, 31). For the Na,K-ATPases, there are human mutations in the residue corresponding to G358 in ATP1A3 and ATP1A2 (multiple different substitutions) (32–36). In Darier disease in the Ca^{2+}-ATPase SERCA2a (ATP2A2), there are R750Q and R750W mutations (37–39). Note that the arginine codon in the Na,K-ATPases is CGC, while that in ATP2A2 is CGG. Certain single base missense mutations could result in substitution with leucine, proline, or glycine for either ATPase, but others will result in tryptophan in SERCA2 *versus* cysteine in Na,K-ATPase and glutamine in SERCA2 *versus* histidine in Na,K-ATPase. Substitution to serine is only possible for the Na,K-ATPases. Proline, glycine, and serine clinical variants have not been reported so far.

The human arginine mutations in ATP1A2 and ATP2A2 have not been reported to produce notable fever sensitivity. In fact, ATP1A2's R763H was identified in a large hemiplegic migraine family first described in 1997 (26, 40). Typical migraine triggers were reported in all subjects, and minor head trauma was a trigger in 83% of subjects, but fever was not mentioned. It is possible that fever has similar effects on ATP1A2 stability in glia, but that manifestations are subclinical because glial function is not as impaired as neuronal function. As for the Ca^{2+}-ATPase ATP2A2, it is typical for the skin condition in Darier disease patients to worsen in heat and humidity and for severe flare-ups to be accompanied by high fever (41), but whether these reflect causation or side-effects is unknown.

Mechanistic investigations in other P-type ATPases

The electrogenic transport properties of R763H in human ATP1A2 were studied by voltage-clamp electrophysiology in *Xenopus* oocytes (42) with findings that complement the present functional studies. Protein level was not obviously reduced, but the oocytes had been incubated at 18 °C. Pump current of R763H was reduced by ∼2/3, and so estimated turnover number was reduced, and kinetic constants for K^+ and Na^+ dependence of transient currents at room temperature changed in the same directions as here, albeit with smaller changes (note, however, that the electrophysiological measurements determined the apparent Na^+ affinity on the

extracellular side, whereas the present data refer to the intracellular side, where Na^+ is more critical for activity). The results are as consistent as could be expected given the difference in experimental temperatures and conditions.

Another study utilized mutagenized *Drosophila* that had been screened for mutations causing temperature-sensitive discoordination (43). In one strain, an A617T mutation in *drosophila* SERCA was found, corresponding to the A606T FHM2 mutation in ATP1A2 and to A599T in ATP1A3. NIH3T3 cells transiently expressing the corresponding A616T in mouse SERCA2 had normal intracellular calcium stores, but stores were emptied after cells were heated to 42 °C for 30 min. A leak of Ca^{2+} through the Ca^{2+}-ATPase caused by mutation only at elevated temperature was considered a possible cause. To extend the findings, transgenic flies were generated that expressed another pathogenic SERCA mutation, *drosophila* SERCA R751Q, which the investigators knew corresponds to Darier disease ATP1A2 mutation R750Q. Those flies also showed temperature-sensitive discoordination. In NIH3T3 cells, transient R750Q expression elicited some calcium store emptying even without heating and complete emptying after heating (43).

The apparent Ca-ATPase leakiness might seem to parallel the temperature-sensitivity of R756H reported here after longer incubations at 39 °C. There is a fundamental cell biological difference between SERCA and Na,K-ATPase, however. There is no recognized role for Na and K transport in the ER. In contrast, both SERCAs are necessary components of the secretory pathway: they accumulate the lumenal calcium that is essential for normal protein biosynthesis and for signaling *via* Ca^{2+} release. Importantly, the SERCA inhibitor thapsigargin also empties the calcium store (44). However, the authors found support for the leakiness mechanism by testing the same mutations in yet another P-type ATPase, the plasma membrane Ca-ATPase, ATP2B1. Mutation of A617T and R869Q, the corresponding residues, elevated cytoplasmic Ca^{2+} at 37 °C modestly, but much more at 39 °C or 42 °C (43). The magnitude was comparable to the effect of ionomycin.

A confounding observation in (43) was that in SERCA2, a mutation at the ATP binding site in the cytoplasmic N domain and a mutation in the cytoplasmic A domain also emptied the Ca^{2+} stores during heating. The same ATP-site mutation introduced into the plasma membrane Ca^{2+}-ATPase also increased Ca^{2+} influx after heating. In P-type ATPases, the N and A domains are involved in rigid body movements during ion transport that act by altering the conformation of another cytoplasmic domain, the P domain, and have no direct contact with the membrane domain. Thus, it is unexpected if their N and A domain mutations caused leakiness. It remains unknown whether the loss of Ca^{2+} stores would also result from the pathologies we observed in Na,K-ATPase: some impairment of biosynthesis, temperature-dependent irreversible inactivation, internalization, and degradation, on top of the broader cellular damage of elevated temperature. Leakiness seems unlikely for R756H ATP1A3 because of cell recovery from heating and because of long-term survival when the endogenous Na,K-ATPase is inhibited with ouabain. An answer to the question whether any of the mutations caused a leak will require a more biophysical approach.

Cell biological effects of R756H mutation

Even during growth at 37 °C, there was reduced expression of the α3 subunit of R756H, and it was further reduced at 39 °C. The presence of some β subunit with immature glycosylation demonstrates that α3-β complexes were retained in the ER for a period of time, while the ability of the mutant Na,K-ATPase to support cell life when the endogenous α1 is inhibited with ouabain demonstrates that the complex does reach the plasma membrane. This was borne out by immunofluorescence localization and is typical of the scenario where misfolding during biosynthesis is recognized by ER chaperones (45) and managed by the successive addition and cleavage of glucose residues on N-linked glycoconjugates until the protein is ready to transit to the Golgi apparatus (46). When α3 decreased at 39 °C, α1 increased with no net change in β subunit. A return to 37 °C resulted in replacement synthesis of α3. Immunofluorescence showed both reduction of the R756H mutant protein and aggregation within the cell. A lysosome marker showed dispersion of lysosomes throughout the cytoplasm of R756H-expressing cells after 24 h at 39 °C and blockade by CQ, which blocks the fusion of endosomes with lysosomes. These data paint a picture of a protein with mildly impaired biosynthesis and a significant loss of thermal stability after it traffics to the plasma membrane.

Experimental procedures

DNA constructs and site-directed mutagenesis

For the Flp-In system in 293 cells, a DNA construct containing 3.5 kb of ATP1A3 full-length cDNA (GenBank accession NM_152296.4) was purchased from OriGene. 3042 bp of ATP1A3 ORF fragment was PCR-amplified using primers 5′-aaaAAGCTTggccacc-ATGGGGGACAAGAAAGATG (forward) and 5′-aaaGGATCCTCAGTAGTAGGTTTCCTTC (reverse) and subcloned in pcDNA5/FRT/TO vector using HindIII and BamHI restriction sites to produce pcDNA5/FRT/TO/ATP1A3-OR (ouabain resistant) for Tet-inducible expression in Flp-in 293 cell lines (ThermoFisher Scientific). Site-directed mutagenesis by PCR was performed to generate mutations including D366H, R463C, S729Y, D742Y, D743H, R756C, R756H, R756L, E815K, E818K, D923N, and L924P using pcDNA5/FRT/TO/ATP1A3-OR. The subcloning and site-directed mutagenesis were performed by Mutagenex (now Molecular Biology Core, The Ohio State University, Department of Surgery). All constructs were confirmed by Sanger sequencing for whole ORF sequences. For COS-1 cells, plasmids were mutagenized by PCR using the quick-change mutagenesis kit (11, 47).

Stable cell transfection and growth

For cell biology experiments, Na,K-ATPase α3 subunit (ATP1A3) was expressed using the Flp-In system in 293 cells, where recombination of a plasmid vector containing the cDNA with and without mutation occurs at a single FRT site, as

previously described (1). Stable cell lines were obtained by hygromycin selection, and expression was controlled with tetracycline. This single-copy insertion ensures that expression levels are moderate and consistent from mutation to mutation to enable comparisons of the posttranscriptional expression and properties of different mutations (1). Baseline incubator temperature was set to 36.6 °C to minimize stress from opening-related fluctuations. Ouabain, CQ, and 4-phenylbutyrate were from Sigma, and lactacystin and cycloheximide are from Cayman Chemicals.

For analysis of changes in enzyme properties, large-scale preparations were made from transfectants of COS-1 cells; stable cell lines obtained by ouabain selection, where inhibition of the endogenous ATP1A1 results in a requirement for sufficient Na,K-ATPase activity of the transfected ATP1A3 to support cell growth (11). Transfection, growth, and ouabain selection of COS-1 cells were performed as previously described (47). These cultures were grown for months to optimize yield for biochemical assays.

In both cell lines, the WT and mutations were expressed from a plasmid where α3 carries two mutations in the first extracellular loop (Q108R and N119D), originally found in the ouabain-resistant rat, that reduce the affinity for ouabain (10). This allows a practical assessment of loss of activity in the mutant when a low concentration of ouabain is included during growth to inactivate the endogenous α1. Many pathogenic Na,K-ATPase mutations inactivate the exogenous Na,K-ATPase and the cells die, but if there is at least ∼10% residual activity, the cells survive and grow in low ouabain (12). In our hands, R756H-expressing 293 Flp-In and COS-1 cells survived when tested at 3 μM and 5 μM ouabain, respectively. The 293 Flp-In lines were cultured continuously with hygromycin selection and the COS-1 lines with ouabain selection. Unlike WT and R756H, mutants R756C and R756L were unable to support growth of 293 and COS-1 cells in the presence of ouabain, indicating that pump activity was below the critical level. In COS-1 cells, the lack of survival of cells transfected with R756C and R756L was confirmed for each mutant in three independent transfection experiments, each using mutant cDNA obtained from three independent mutagenesis reactions. All cDNA constructs were full-length sequenced before transfection, and for the R756H mutant COS-1 cell line, the incorporation of the mutant cDNA was verified by genomic sequencing.

Analysis of protein expression in 293 cells

Methods for production of cell lysates, SDS gel electrophoresis, and Western blotting were as described previously (1). Antibodies used here included α3-specific goat polyclonal antibody C16 or mouse monoclonal antibody clone F1 raised against the same peptide (from Santa Cruz Biotechnology). α1-specific monoclonal antibody 6F (Developmental Studies Hybridoma Bank, University of Iowa) or M17-P5-F11 [gift of Dr W. James Ball, University of Cincinnati, (48)] were used to detect human α1 and β1 subunits. Other antibodies used were rabbit anti-HSP70 4872, rabbit mAb anti-BiP C50B12 (3177), rabbit mAb anti-LC3 E7X4S, and HRP-conjugated rabbit mAb anti-GAPDH D16H11 from Cell Signaling Technology.

Functional analysis of COS-1 cell-expressed enzyme

The plasma membrane fractions of COS-1 cells containing the expressed WT or mutant R756H were isolated by differential centrifugation and made leaky with alamethicin to allow Na^+, K^+, and ATP to bind to the Na,K-ATPase from both sides of the membrane (11, 47). Functional analysis was carried out on the leaky membranes. The composition of the media is described in the figure legends. ATPase activity during a 15 min incubation was determined by following the liberation of P_i at 37 °C (11). The ouabain concentration was 10 μM to inhibit the endogenous COS-1 cell Na,K-ATPase. For background subtraction, similar measurements were carried out in the presence of 10 mM ouabain, inhibiting all Na,K-ATPase activity.

The Na^+ dependence of phosphorylation was determined by incubating the membranes for 10 s at 0 °C with 2 μM [γ-^{32}P] ATP in the presence of varying concentrations of Na^+ and oligomycin (to block dephosphorylation) and ouabain to inhibit the endogenous Na,K-ATPase. Acid quenching of the phosphoenzyme, isolation of Na,K-ATPase protein by SDS-PAGE at pH 6.0 was performed as before (11), and quantification of the associated radioactivity was obtained by phosphorimaging using a Cyclone Storage Phosphor System (PerkinElmer Life Sciences).

Thermal inactivation was studied by incubating the leaky COS-1 cell membrane preparation containing WT or mutant R756H in the media described in the figure legend in a thermostated water bath at 37 °C, 39 °C, or 41 °C. After various time intervals samples were withdrawn for test of the ATPase activity at 37 °C under the same conditions as for the maximal turnover rate in Figure 2*B*.

Immunofluorescence

Cells were grown in 8-well chamber Lab-Tek Pernox slides. They were fixed with 4% paraformaldehyde-lysine-periodate (49) treated with 1% SDS in PBS for antigen retrieval and blocked in 1% bovine serum albumin in PBS supplemented with 0.2% Triton X-100. The α3 subunit was stained with a goat polyclonal antibody (Santa Cruz, C16) followed by donkey-anti-goat Alexa-fluor 555. The β1 subunit was stained by mouse monoclonal antibody M17-P5-F11 followed by rabbit-anti mouse Alexa-fluor 488 (Life Technologies). LAMP1 was stained with rabbit mAb D2D1 (9091) (Cell Signaling Technology), followed by goat-anti-rabbit Alexa-Fluor 555. Images were obtained on an Olympus BX60 fluorescence microscope.

Analysis of structures

The Na^+ form (PDB file 3WGU) has three Na^+ bound in the occluded ion binding site, ADP, and AlF_4^- as a phosphate analog (50). It is the only structure with resolution of the N terminus of the β subunit. The "ground state" (PDB file 7DDF) was crystallized with Mg^{2}+ and BeF_3^- as a phosphate analog

(51). The K^+ form (PDB file 3KDP) has two bound K^+ and MgF_4^{2-} as a phosphate analog (52). The structure of SERCA2 (PDB file 6LN5) was crystallized in Ca^{2+} and AMPPCP.

Structures were studied in the Swiss PDB Viewer version 4.1 (53). Putative hydrogen bonds (*black dashed lines*) were calculated in Swiss PDB Viewer 4.1 as determined by both distance and angle. Amino acid substitutions and their rotamers were investigated with the Mutate function. Alignments were made with Magic Fit in Swiss PDB viewer.

Data availability

All of the data are within the paper.

Acknowledgments—We thank Randi Scheel, Aarhus University, for expert technical assistance, Anja P. Einholm for her initial contribution to Figure 2, and the foundations Hope for Annabel and CureAHC for their support and commitment.

Author contributions—E. A., L. J. O., A. B., B. V., and K. J. S. conceptualization; E. A., M. S.T.-J., R. H., J.-K. K., K. E. L., P. F., and K. J. S. investigation; E. A., M. S. T.-J., R. H., B. V., and K. J. S. formal analysis; E. A., J.-K. K., L. J. O., B. V., and K. J. S. resources; E. A., J.-K. K., B. V., and K. J. S. writing—original draft; J.-K. K., L. J. O., A. B., B. V., and K. J. S. funding acquisition; L. J. O. and A. B. writing-reviewing and editing.

Funding and additional information—This work was supported by NIH grant NS058949 to A. B.; by grants from The Danish Council for Independent Research (grant DFF 7016–00193B) and The Lundbeck Foundation (grant R223–2016–595) to B. V.; by a research startup fund from the Department of Surgery, the College of Medicine, The Ohio State University (FD100 FY2019–2022) to J.-K.K.; and by grants from CureAHC and Hope for Annabel to K. J. S. The content is solely the responsibility of the authors and does not necessarily represent the official views of the National Institutes of Health.

Conflict of interest—E. A., M. S. T-J., R. H., J. J-K., K. E. L., P. F., L. J. O., B. V., and K. J. S. declare no competing financial interests. A. B. serves the McKnight Brain Research Foundation as a trustee and is on the board of directors of the American Board of Psychiatry and Neurology and Care Directions.

Abbreviations—The abbreviations used are: CQ, chloroquine; RDP, rapid-onset dystonia-parkinsonism; AHC, alternating hemiplegia of childhood; LAMP1, lysosomal-associated membrane protein 1; ER, endoplasmic reticulum; SERCA, sarcoplasmic-endoplasmic reticulum Ca^{2+}-ATPase; UPR, unfolded protein response.

References

1. Arystarkhova, E., Haq, I. U., Luebbert, T., Mochel, F., Saunders-Pullman, R., Bressman, S. B., *et al.* (2019) Factors in the disease severity of *ATP1A3* mutations: impairment, misfolding, and allele competition. *Neurobiol. Dis.* **132**, 104577
2. Lazarov, E., Hillebrand, M., Schroder, S., Ternka, K., Hofhuis, J., Ohlenbusch, A., *et al.* (2020) Comparative analysis of alternating hemiplegia of childhood and rapid-onset dystonia-parkinsonism ATP1A3 mutations reveals functional deficits, which do not correlate with disease severity. *Neurobiol. Dis.* **143**, 105012
3. Arystarkhova, E., Ozelius, L. J., Brashear, A., and Sweadner, K. J. (2021) Misfolding, altered membrane distributions, and the unfolded protein response contribute to pathogenicity differences in Na,K-ATPase *ATP1A3* mutations. *J. Biol. Chem.* **296**, 100019
4. Toyoshima, C., Nakasako, M., Nomura, H., and Ogawa, H. (2000) Crystal structure of the calcium pump of sarcoplasmic reticulum at 2.6 Å resolution. *Nature* **405**, 647–655
5. Jorgensen, P. L., Hakansson, K. O., and Karlish, S. J. D. (2003) Structure and mechanism of Na,K-ATPase: Functional sites and their interactions. *Ann. Rev. Physiol.* **65**, 817–849
6. Clausen, M. V., Hilbers, F., and Poulsen, H. (2017) The structure and function of the Na,K-ATPase isoforms in health and disease. *Front. Physiol.* **8**, 371
7. Beguin, P., Hasler, U., Beggah, A., Horisberger, J. D., and Geering, K. (1998) Membrane integration of Na,K-ATPase α-subunits and β subunit assembly. *J. Biol. Chem.* **273**, 24921–24931
8. Tokhtaeva, E., Sachs, G., and Vagin, O. (2009) Assembly with the Na,K-ATPase α1 subunit is required for export of β1 and β2 subunits from the endoplasmic reticulum. *Biochemistry* **48**, 11421–11431
9. Molinari, M. (2007) N-glycan structure dictates extension of protein folding or onset of disposal. *Nat. Chem. Biol.* **3**, 313–320
10. Price, E. M., Rice, D. A., and Lingrel, J. B. (1990) Structure-function studies of Na,K-ATPase. Site-directed mutagenesis of the border residues from the H1-H2 extracellular domain of the alpha subunit. *J. Biol. Chem.* **265**, 6638–6641
11. Roenn, C. P., Li, M., Schack, V. R., Forster, I. C., Holm, R., Toustrup-Jensen, M. S., *et al.* (2019) Functional consequences of the CAPOS mutation E818K of Na^+,K^+-ATPase. *J. Biol. Chem.* **294**, 269–280
12. Holm, R., Toustrup-Jensen, M. S., Einholm, A. P., Schack, V. R., Andersen, J. P., and Vilsen, B. (2016) Neurological disease mutations of α3 Na^+,K^+-ATPase: structural and functional perspectives and rescue of compromised function. *Biochim. Biophys. Acta* **1857**, 1807–1828
13. Cherniavsky-Lev, M., Karlish, S. J., and Garty, H. (2015) Cardiac glycosides induced toxicity in human cells expressing alpha1-, alpha2-, or alpha3-isoforms of Na-K-ATPase. *Am. J. Physiol. Cell Physiol.* **309**, C126–C135
14. Bernhem, K., Blom, H., and Brismar, H. (2018) Quantification of endogenous and exogenous protein expressions of Na,K-ATPase with super-resolution PALM/STORM imaging. *PLoS.One.* **13**, e0195825
15. Einholm, A. P., Toustrup-Jensen, M. S., Holm, R., Andersen, J. P., and Vilsen, B. (2010) The rapid-onset dystonia parkinsonism mutation D923N of the Na^+,K^+-ATPase α3 isoform disrupts Na^+ interaction at the third Na^+ site. *J. Biol. Chem.* **285**, 26245–26254
16. Shoshani, L., Contreras, R. G., Roldan, M. L., Moreno, J., Lazaro, A., Balda, M. S., *et al.* (2005) The polarized expression of Na+,K+-ATPase in epithelia depends on the association between beta-subunits located in neighboring cells. *Mol. Biol. Cell* **16**, 1071–1081
17. Vagin, O., Tokhtaeva, E., and Sachs, G. (2006) The role of the β1 subunit of the Na,K-ATPase and its glycosylation in cell-cell adhesion. *J. Biol. Chem.* **281**, 39573–39587
18. Mauthe, M., Orhon, I., Rocchi, C., Zhou, X., Luhr, M., Hijlkema, K. J., *et al.* (2018) Chloroquine inhibits autophagic flux by decreasing autophagosome-lysosome fusion. *Autophagy* **14**, 1435–1455
19. Zhang, W., Li, J., Zhuo, X., Zhou, J., Feng, W., Gong, S., *et al.* (2022) Chinese patients with p.Arg756 mutations of ATP1A3: clinical manifestations, treatment, and follow-up. *Pediatr. Investig.* **6**, 5–10
20. Sorensen, T. L., and Andersen, J. P. (2000) Importance of stalk segment S5 for intramolecular communication in the sarcoplasmic reticulum Ca2+-ATPase. *J. Biol. Chem.* **275**, 28954–28961
21. Miles, A. J., Wallace, B. A., and Esmann, M. (2011) Correlation of structural and functional thermal stability of the integral membrane protein Na,K-ATPase. *Biochim. Biophys. Acta* **1808**, 2573–2580
22. Grinberg, A. V., Gevondyan, N. M., Grinberg, N. V., and Grinberg, V. Y. (2001) The thermal unfolding and domain structure of Na+/K+-exchanging ATPase. A scanning calorimetry study. *Eur. J. Biochem.* **268**, 5027–5036
23. Demos, M. K., van Karnebeek, C. D. M., Ross, C. J. D., Adam, S., Shen, Y., Zhan, S. H., *et al.* (2014) A novel recurrent mutation in *ATP1A3* causes CAPOS syndrome. *Orph. J. Rare Dis.* **9**, 15

24. Prontera, P., Sarchielli, P., Caproni, S., Bedetti, C., Cupini, L. M., Calabresi, P., *et al.* (2018) Epilepsy in hemiplegic migraine: genetic mutations and clinical implications. *Cephalalgia* **38**, 361–373
25. Hasday, J. D., Thompson, C., and Singh, I. S. (2014) Fever, immunity, and molecular adaptations. *Compr. Physiol.* **4**, 109–148
26. Gardner, K., Estevez, M., Keryanov, S., Estevez, A., Barmada, M., Badger, J., *et al.* (2004) A two-locus FHM2 family with unique *ATP1A2* mutation and comparative study in *C. elegans* showing regulation of tryptophan hydroxylase by EAT-6 and UNC-2, the orthologus *FHM2* and *FHM1* genes. *Cephalalgia* **24**, 147–152
27. Jurkat-Rott, K., Freilinger, T., Dreiser, J. P., Herzog, J., Göbel, H., Petzold, G. C., *et al.* (2004) Variability of familial hemiplegic migraine with novel A1A2 Na^+/K^+-ATPase variants. *Neurology* **62**, 1857–1861
28. Thomsen, L. L., Kirchmann, M., Bjornsson, A., Stefansson, H., Jensen, R. M., Fasquel, A. C., *et al.* (2007) The genetic spectrum of a population-based sample of familial hemiplegic migraine. *Brain* **130**, 346–356
29. Nagai, A., Tanaka, D., Kuroshima, K., Ura, S., Yoshida, K., Takahashi, K., *et al.* (2020) Neurovascular changes in magnetic resonance imagining and single-photon emission computed tomography during migraine attack in patients with FHM2 mutations. *Cephalalgia Rep.* **3**, 1–4
30. Riant, F., De Fusco, M., Aridon, P., Ducros, A., Ploton, C., Marchelli, F., *et al.* (2005) ATP1A2 mutations in 11 families with familial hemiplegic migraine. *Hum. Mutat.* **26**, 281
31. Jen, J. C., Klein, A., Boltshauser, E., Cartwright, M. S., Roach, E. S., Mamsa, H., *et al.* (2007) Prolonged hemiplegic episodes in children due to mutations in *ATP1A2*. *J. Neurol. Neurosurg. Psych.* **78**, 523–526
32. Panagiotakaki, E., De Grandis, E., Stagnaro, M., Heinzen, E. L., Fons, C., Sisodiya, S., *et al.* (2015) Clinical profile of patients with *ATP1A3* mutations in Alternating Hemiplegia of Childhood-a study of 155 patients. *Orphanet. J. Rare. Dis.* **10**, 123
33. Paciorkowski, A. R., McDaniel, S. S., Jansen, L. A., Tully, H., Tuttle, E., Ghoneim, D. H., *et al.* (2015) Novel mutations in *ATP1A3* associated with catastrophic early life epilepsy, episodic prolonged apnea, and postnatal microcephaly. *Epilepsia* **56**, 422–430
34. Pereira, P., Guerreiro, A., Fonseca, M., Halpern, C., Pinto-Basto, J., and Monteiro, J. P. (2015) A distinct phenotype in a novel ATP1A3 mutation: connecting the two ends of a spectrum. *Mov. Disord. Clin. Prac.* https://doi.org/10.1002/mdc3.12263
35. Liu, J., Tong, L., Song, S., Niu, Y., Li, J., Wu, X., *et al.* (2018) Novel and *de novo* mutations in pediatric refractory epilepsy. *Mol. Brain* **11**, 48
36. Heyne, H. O., Singh, T., Stamberger, H., Abou, J. R., Caglayan, H., Craiu, D., *et al.* (2018) *De novo* variants in neurodevelopmental disorders with epilepsy. *Nat. Genet.* **50**, 1048–1053
37. Mac Manus, M. P., Cavalleri, G., Ball, D. L., Beasley, M., Rotstein, H., and McKay, M. J. (2001) Exacerbation, then clearance, of mutation-proven Darier's disease of the skin after radiotherapy for bronchial carcinoma: a case of radiation-induced epidermal differentiation? *Radiat. Res.* **156**, 724–730
38. Ikeda, S., Mayuzumi, N., Shigihara, T., Epstein, E. H., Jr., Goldsmith, L. A., and Ogawa, H. (2003) Mutations in ATP2A2 in patients with Darier's disease. *J. Invest. Dermatol.* **121**, 475–477
39. Dodiuk-Gad, R. P., Cohen-Barak, E., Khayat, M., Milo, H., Amariglio-Diskin, L., Danial-Faran, N., *et al.* (2016) Darier disease in Israel: combined evaluation of genetic and neuropsychiatric aspects. *Br. J. Dermatol.* **174**, 562–568
40. Gardner, K., Barmada, M. M., Ptacek, L. J., and Hoffman, E. P. (1997) A new locus for hemiplegic migraine maps to chromosome 1q31. *Neurology* **49**, 1231–1238
41. Munro, C. S. (1992) The phenotype of Darier's disease: penetrance and expressivity in adults and children. *Br. J. Dermatol.* **127**, 126–130
42. Tavraz, N. N., Friedrich, T., Durr, K. L., Koenderink, J. B., Bamberg, E., Freilinger, T., *et al.* (2008) Diverse functional consequences of mutations in the Na^+/K^+-ATPase α2-subunit causing familial hemiplegic migraine type 2. *J. Biol. Chem.* **283**, 31097–31106
43. Kaneko, M., Desai, B. S., and Cook, B. (2014) Ionic leakage underlies a gain-of-function effect of dominant disease mutations affecting diverse P-type ATPases. *Nat. Genet.* **46**, 144–151
44. Ghosh, T. K., Bian, J. H., Short, A. D., Rybak, S. L., and Gill, D. L. (1991) Persistent intracellular calcium pool depletion by thapsigargin and its influence on cell growth. *J. Biol. Chem.* **266**, 24690–24697
45. Beggah, A., Mathews, P., Beguin, P., and Geering, K. (1996) Degradation and endoplasmic reticulum retention of unassembled α and β-subunits of Na,K-ATPase correlate with interaction of BiP. *J. Biol. Chem.* **271**, 20895–20902
46. Harada, Y., Ohkawa, Y., Maeda, K., and Taniguchi, N. (2021) Glycan quality control in and out of the endoplasmic reticulum of mammalian cells. *FEBS J.* **289**, 7147–7162
47. Nielsen, H. N., Spontarelli, K., Holm, R., Andersen, J. P., Einholm, A. P., Artigas, P., *et al.* (2019) Distinct effects of Q925 mutation on intracellular and extracellular Na^+ and K^+ binding to the Na^+, K^+-ATPase. *Sci. Rep.* **9**, 13344
48. Sun, Y., and Ball, W. J., Jr. (1994) Identification of antigenic sites on the Na,K-ATPase β-subunit: their sequences and the effects of thiol reduction upon their structure. *Biochim. Biophys. Acta* **1207**, 236–248
49. McLean, I. W., and Nakane, P. K. (1974) Periodate-lysine-paraformaldehyde fixative. A new fixative for immunoelectron microscopy. *J. Histochem. Cytochem.* **22**, 1077–1083
50. Kanai, R., Ogawa, H., Vilsen, B., Cornelius, F., and Toyoshima, C. (2013) Crystal structure of a Na^+-bound Na^+,K^+-ATPase preceding the E1P state. *Nature* **502**, 201–206
51. Kanai, R., Cornelius, F., Ogawa, H., Motoyama, K., Vilsen, B., and Toyoshima, C. (2021) Binding of cardiotonic steroids to Na^+,K^+-ATPase in the E2P state. *Proc. Natl. Acad. Sci. U. S. A.* **118**, e2020438118
52. Morth, J. P., Pedersen, B. P., Toustrup-Jensen, M. S., Sorensen, T. L.-M., Petersen, J., Andersen, J. P., *et al.* (2007) Crystal structure of the sodium-potassium pump. *Nature* **450**, 1043–1049
53. Guex, N., and Peitsch, M. C. (1997) SWISS-MODEL and the Swiss-PdbViewer: an environment for comparative protein modeling. *Electrophoresis* **18**, 2714–2723